Fluorescent and conductive cellulose acetate-based membranes with porphyrins

A. Delgado-Lima [a,*] João P. Borges [b], Isabel M. Ferreira [b], Ana V. Machado [a]

[a] Institute for Polymers and Composites/I3N, University of Minho, Azureím, 4800-0581, Guimarães, Portugal

[b] CENIMAT/I3N, Departamento de Ciência dos Materiais, Faculdade de Ciências e Tecnologia, FCT, Universidade Nova de Lisboa, 2829-516, Caparica, Portugal

Keywords:

Cellulose acetate
Electrospinning
Iridium porphyrins
Electrical conductivity

Abstract

The unique properties of electrospun nanofibers combined with functional compounds allow the preparation of novelty materials that can be employed in a wide range of applications. Among a vast number of polymers, Cellulose Acetate (CA) it is considered easy to electrospun and it was employed as the polymeric matrix, where free and iridium-porphyrins were incorporated. Two different solvent systems were employed according to the porphyrin used, and the best dispersion level on both the electrospun solution and the membranes, was achieved with the iridium porphyrin. The nanofibers with this porphyrin also exhibited electrical properties, while the fluorescence was quenched by the presence of specific axial ligands.

Introduction

Nanofibers prepared by electrospinning with functional compounds, such as metals, semiconductors, ceramics, among others, display specific structural features (phase morphologies and surface topologies) and unique properties that make these materials very interesting from their optical, electronic, photonic, catalytic and magnetic properties. Therefore they gather some of the desired requirements for diverse applications, such as fuel and solar cells, electronic sensors, energy harvesting and storage systems and others [1,2]. Among several candidate compounds, porphyrins and its metallic derivatives are known as important conjugated organic macrocycles with amazing and variable properties and were the chosen compounds to attain the target nanofibers optic/electronic properties [3-10]. The growing interest in these macrocycles combined with the unique features of

the electrospinning technique, such as the nanofiber high specific surface and high aspect ratio, with the possibility of making materials with optic/electronic properties, has generated an increasing interest among researchers in the last decade. For example, nanofibers with fluorescence sensing properties able the rapid detection of 2,4,6-trinitrotoluene trinitro- toluene (TNT) [11], hydrogen chloride (HCl) gas [12], and towards nitroaro-matic explosives [13], were prepared from polymer/porphyrin conjugation. PCL-Porphyrin and PCL-Metalloporphyrin(Zn) electrospun nanofibers were prepared as a fluorescent chemosensor for detection of histamine [8] and poly(N-vinylpyridine)/porphyrin derivatives [14,15]. Electrospun platinum(II) and palladium(II) metalloporphyrins were also employed as optical chemical sensors with a remarkably enhanced dynamic response when compared to compact films [16,17]. Also copolymers of poly(acrylonitrile) with iron-porphyrin or a diamino-substituted porphyrin were successfully electrospun into nanofibers [18,19]. The first porphyrin act as a photosensitizer and in conjugation with TiO_2 particles showed photocatalytic activities in the photodegradation of methyl red [19], while the second showed a great potential to applications in chemical sensors, molecular wires, and photoresponsive materials [18]. Nanofibers composed of polystyrene with encapsulated or bounded porphyrins showed also excellent photophysical properties with a strong antibacterial effect [20,21]. The electrospun of cellulose acetate (CA) has already been extensively studied and several research papers have been published [22-30]. Although there are some works on the electrospinning of polymers with porphyrins, none of them uses the cellulose acetate combined with 5,10,15,20-tetrakis(*p*-tolyl)porphyrin (TTP) or its derivative replaced with iridium TTPIr, which is a metal with very high efficiency to visible light harvesting. Thus, this work will investigate the combination of TTP and TTPIr to develop materials based on biodegradable polymers with optic/electronic properties. Therefore, prior to the preparation of the nanofibers the Hildebrand and Flory-Huggins parameters were predicted and the viscosity and surface tension of the respective solutions were studied. CA and CA containing porphyrins were electrospun and the obtained membranes formed of nanofibers were characterized in terms of morphology, topography, fluorescence, chemistry, thermal stability and electrical conductivity.

Materials and methods

Materials

The cellulose acetate with an acetylation degree of 39.8wt% and the porphyrin 5,10,15,20-tetrakis(*p*-tolyl)porphyrin (TTP) (purity 98%) were acquired from Sigma-Aldrich and their structural formula is represented in Fig. 1. The respective metallated porphyrin (TTPIr) was synthesized according to the literature [31] (Fig. 1c). The free-base TTP ($150mg, 0.22mmol$) and the dimer $[Ir(COD)Cl]_2$ ($225.3mg, 0.33mmol$) were added in xylene and refluxed for 4 days. The solution was purified through column chromatography and the metalloporphyrin was isolated with 70.7% yield, respectively. The solvents employed in this work were acetone (Ac), dichloromethane (DCM), ethanol (Et) and dimethylacetamide (DMAc), purchased from Sigma-Aldrich and used without further purification.

Preparation of the CA solutions

The CA solutions for electrospinning were always prepared using mixed-solvent systems at room temperature with fixed concentrations of 10 and 12wt% of CA. Considering the solutions prepared from CA and porphyrins, both the TTP and the TTPIr were fixed at 5wt% relatively to CA. The systems of solvents employed to prepare the solutions were designated as A and B , where A corresponds to the mixed-solvents DCM/Et in a ratio of 80/20(w/w) and *B* to the solvent system constituted by DCM/Et/DMAc, where the DMAc solvent was fixed at 10wt% relatively to the remaining solvents (DCM and Et). The spinning solutions were obtained after at least 10 h stirring

Preparation of membranes

The membranes were prepared using an electrospinning apparatus, where the previously prepared solutions were placed in a plastic syringe of 1 mL (inner diameter = 4.50 mm) with a tip caliber of 25 G (inner diameter = 0.61 mm). This set was fixed horizontally on the syringe pump (KdScientific KD100) and all the air was manually removed from the solution in the syringe to guarantee the absence of air bubbles that can cause fiber defect. The tip of the syringe was connected to a high-voltage DC power supplier (Glassman High Voltage Inc.) that generated a positive DC voltage, while the grounded counter electrode was connected to a stationary aluminum foil collector. An auxiliary electrode with a ring shape (at the same potential as the syringe tip) was used to control the electrospun area and to ensure that no fibers were deposited outside the designed collector. The electrospinning conditions used to prepare the membranes are listed in Table 1, being the membranes of CA and CA with porphyrins electrospun under the same conditions. The electrospinning process was carried out in a closed acrylic box at a temperature of approximately 22°C and relative humidity of 45%. After processing all the membranes were dried at 80°C for about 12 h .

Characterization of the solutions and membranes

The viscosity was measured under steady state shear flow in a shear rate range from 0.01 to 1000 s^{-1} using a stress-controlled

Table 1
Electrospinning conditions.

Solutions	Solvent System [wt%]	Electrospinning Conditions			
		Q(mL/h)	d(cm)	DV(kV)	t (min)
CA10(A) CA12(A) CA10+TTP(A) CA12+TTP(A)	DCM/Et [80/20]	0.5	15	16	10
CA10(B) CA12(B) CA10+TTPIr(B) CA12+TTPIr(B)	DCM/Et/DMAc [72/18/10]	0.1	15	20	60

Q = flow rate; d = tip-to-collector distance; DV = applied voltage; t = time. rheometer Bohlin Gemini HR nano, with a cone-plate geometry (20 mm diameter and 2°) at room temperature. A solvent trap was used during measurements in order to avoid solvent evaporation.

The surface tension of the electrospinning solutions was studied using a KSV NIMA Langmuir and Langmuir-Blodgett Troughs (KSV NIMA L & LB Troughs) at room temperature (approximately 20°C). The surface tension of 1.8 mL aliquots (x 3) was obtained by the difference of the surface tension between the aliquot and the reference value of water 72.75mN/m [32].

The membranes were analyzed by FTIR spectroscopy with a FTIR4100-Jasco in the range of $4000 - 500\ cm^{-1}$ with an attenuated total reflectance accessory (ATR) using a resolution of $8\ cm^{-1}$ with 64 repetitions scans average per sample. For comparison the TTP and TTPIr powder were compressed into KBr pellets and analyzed in the transmittance mode using the same parameters. All the samples, including the membranes, were previously dried. Raman and emission spectroscopy were carried out on a LabRAM HR Evolution Raman spectrometer (Horiba Scientific, France) coupled with a Horiba Scientific's Labspec 6 spectroscopy suite that provides a complete instrument control and data processing. The Raman spectra were acquired with a 532 nm laser excitation wavelength (0.1% laser intensity), with an acquisition time and accumulation of 30 s in a range between 500 and $1800\ cm^{-1}$, while the emission spectra were collected with the same laser wavelength with 0.01% intensity and an acquisition time and accumulation of 5 s in a range between 300 and 800 nm .

The morphology and the measurement of the fibers diameter (50 fibers/sample) were analyzed by scanning electron microscopy (SEM) on a NanoSEM FEI Nova 200, at an acceleration voltage of $5.00 - 10.00kV$ in second electron image mode coupled to an energy dispersive X-ray (EDAX- Pegasus X4M) spectrometer. Previously to the SEM analysis the samples were sputter coated with a gold/platinum mixture, leaving an uncoated area to perform the EDX analyses. An Olympus BX51 microscope with X-Cite series 120Q fluorescence excitation of ultraviolet, blue and green light was used to observe the membranes at different irradiation light.

Atomic force microscopy was performed in a Keysight 9500 Scanning Probe Microscope, the images were kindly provided by Keysight Linz Company. The system was equipped with the standard 90 mm scanner and the samples were analyzed with the continuous force volume (CFV) mode $k = 2\ N/m$, mod.frequency $= 600\ Hz$, amplitude $= 300\ nm, 0.5\ Hz$ scan speed; (including Current imaging on sample E using CFV mode), and the Kelvin Probe Force Microscopy (KFM) mode $k = 2\ N/m, f = 65kHz$. Additionally, a 2D matrix of fast force sweeps was applied (300-1000 sweeps per second), which allowed the mechanical data measurement (topography). Current data at conventional imaging speeds using the KFM mode were acquired.

Static contact angles were also measured on the sample surface through the sessile drop method using an OCA20 contact

a)

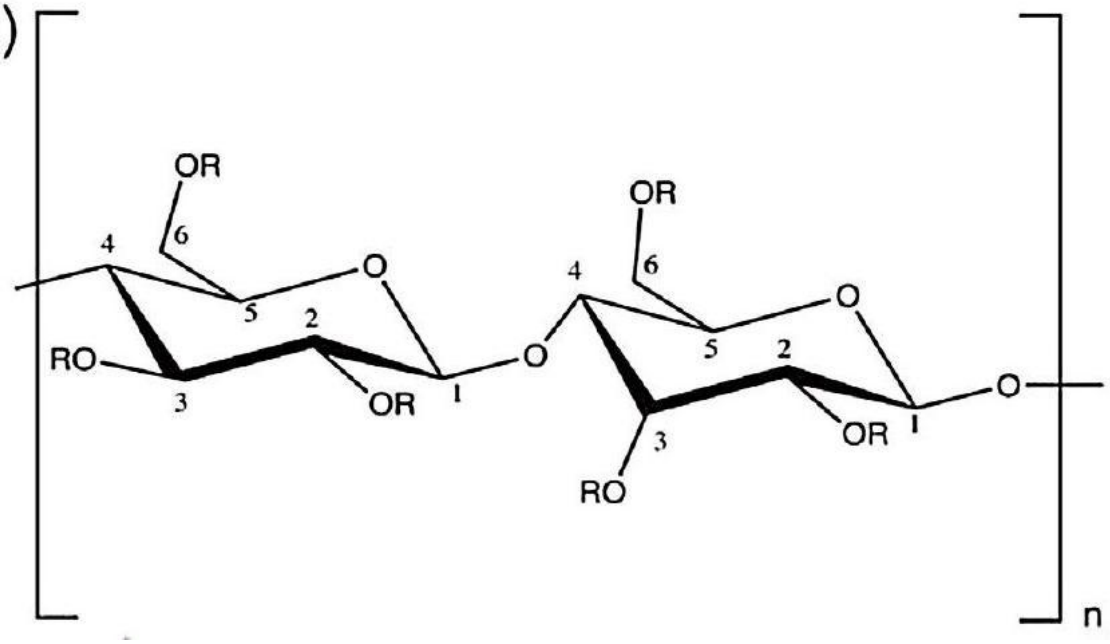

b)

b)

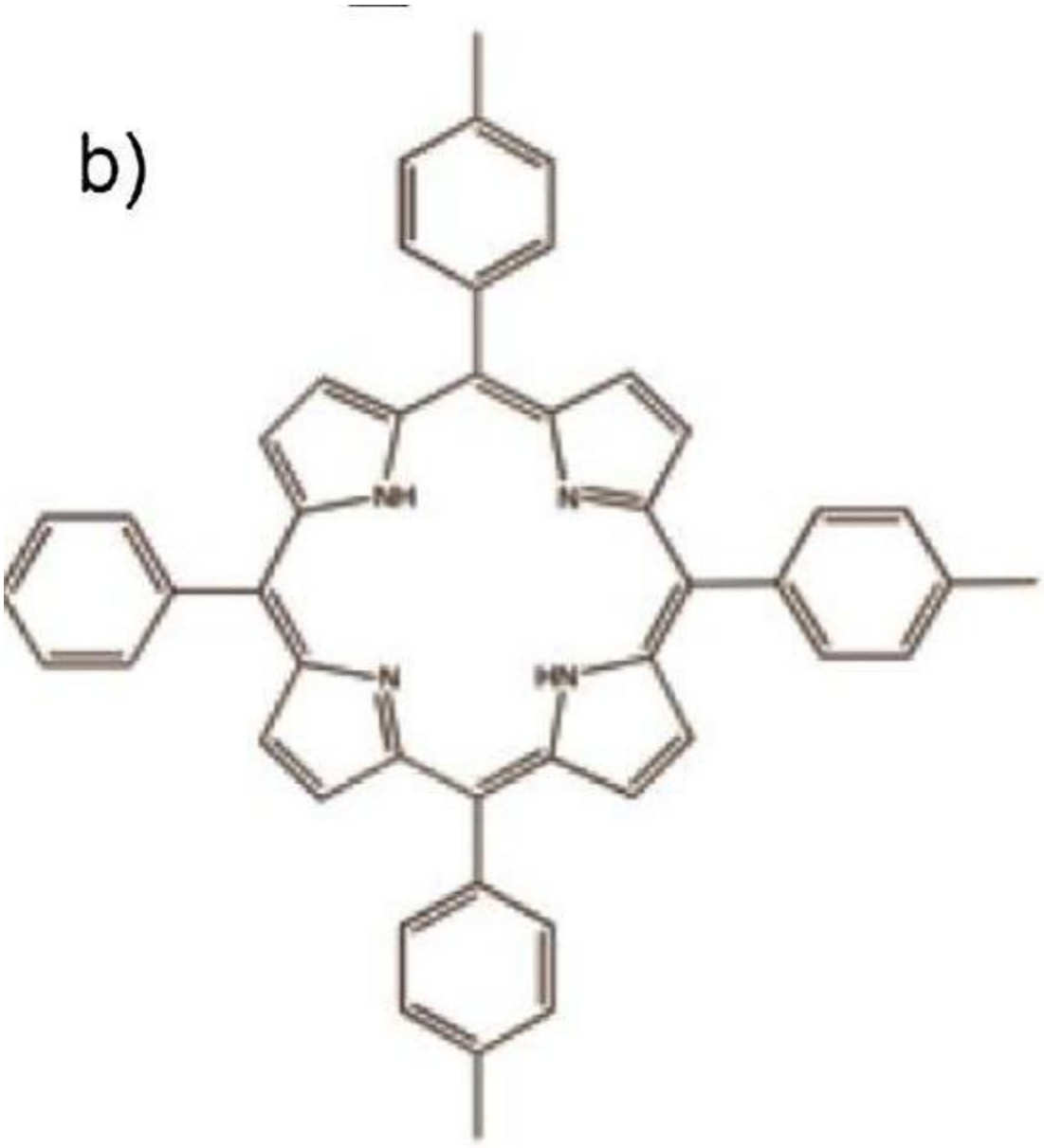

c)

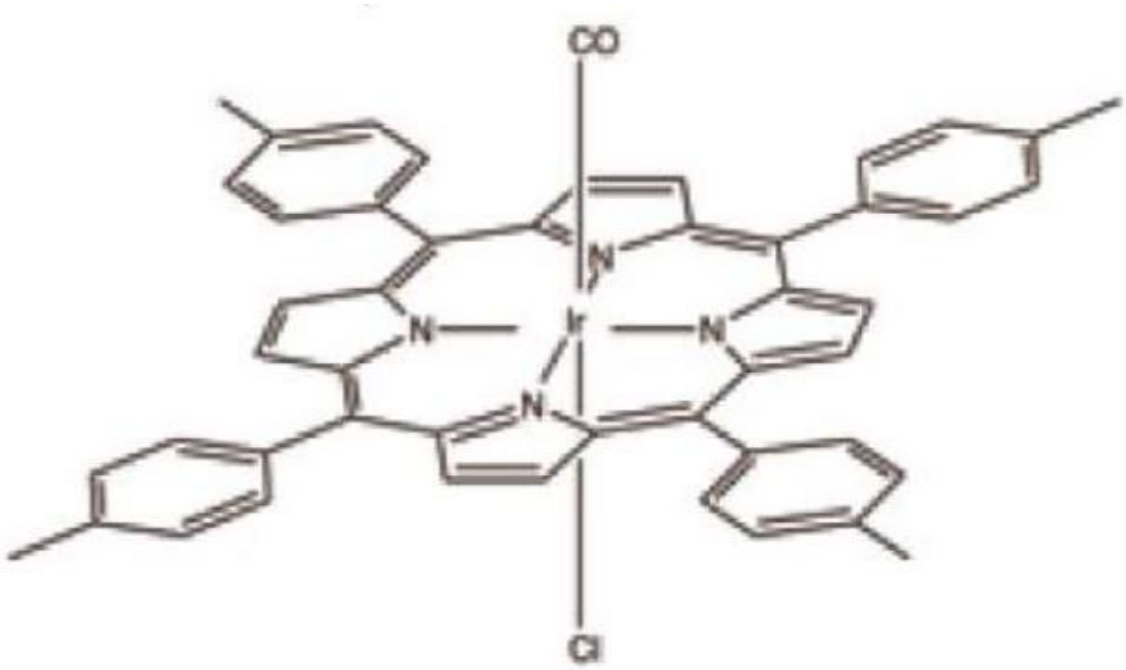

Fig. 1. (a) Cellulose acetate $R = H$ or $R = COCH_3$ (according to acetylation degree); (b) porphyrin TTP and (c) metallated porphyrin TTPIr.
angle instrument (DataPhysics Instruments GmbH, Filderstadt, Germany). Samples were cut in a rectangular specimen with 0.5 × 1 cm. Water microdrops (volume ≈ 5 mL, Milli-Q water) were generated with an electronic micrometric syringe and deposited on the substrate surface according to the so-called pick-up procedure. The contact angle was determined after 5 s of the moment of the drop deposition and settling. Image acquisition, analysis and contact angle determination was performed using the SCA20 v.4.3.12 software (Dataphysics Instruments GmbH, Filderstadt, Germany). A total of five drops of each probe liquid was dispensed and each drop was placed in a different region of the sample. The results correspond to the average and are presented with the respective standard deviations.

The thermal stability of both porphyrins, CA and respective membranes were studied using a TGA Q500 from TA Instruments within a temperature range of $60 - 800°C$ under N_2 atmosphere at a heating rate of $10°C/min$

Results and discussion

Properties of the solutions

According to literature the solvent system Ac/DMAc is one of the most employed to prepare electrospinning solutions of CA [25,26,33,34]. While this solvent was good for CA, when the porphyrins were incorporated in the polymer a suspension of large particles was obtained (independently of the addition order of the components) and the membranes presented sizable defects (large projections of material). To overcome this issue, and in order to choose a different solvent system suitable for both porphyrins and polymer, the Hildebrand (d) and Flory-Huggins (c) parameters were previously estimated. The d of the system of solvents was calculated

considering the overall contribution of each solvent according to equation Equation (1) [35]:

$$\delta = \sum_i \phi_i \delta_i \quad (1)$$

Where ϕ_i corresponds to the volume fraction of the solvent and δ_i is the Hildebrand parameter. d derives from the cohesive energy density of the solvent and it is fundamentally a liquid property value that indicates the relative solvency behavior of a specific solvent [34-36]. Therefore, solvents with similar Hildebrand values are miscible, once they have an identical cohesive energy that allows mixing [35,36]. The Flory-Huggins parameter (c), which only considers the solvent interaction, complements this analysis by indicating which solvent is thermodynamically more stable for a specific polymer [35,37,38]. Thus, lower c values suggest that the solvent is favorable to dissolve the polymer. Even though, these calculations only take into account the solvents and the polymer, since no data is available for these porphyrins, the results provide a good approach to predict an appropriate system of solvents. The Ac/DMAc solvent system was then substituted by two different systems, DCM/Et, with a d of $21.4 MPa^{1/2}$ and DCM/Et/DMAc with a d of $21.5 MPa^{1/2}$ (Table 2). These showed to be suitable solvents to dissolve CA, since it is known that this polymer is ideally soluble in solvents or system of solvents with Hildebrand parameters between 19.43 and $25.57 MPa^{1/2}$ [34,37]. Since the c values of CA and of solvents DCM and EtOH were not found in literature, it was possible to predict a relationship based on similar molecules, such as chloroform ($CHCl_3$) and methanol (CH_3OH), respectively (Table 2). Thereby the interaction CA - solvents can be organized according the following order: c(DMAc) ≈ c(DCM) « c(EtOH), showing that the DMAc and DCM solvents are thermodynamically more stable for CA and ethanol acts as a non-solvent.

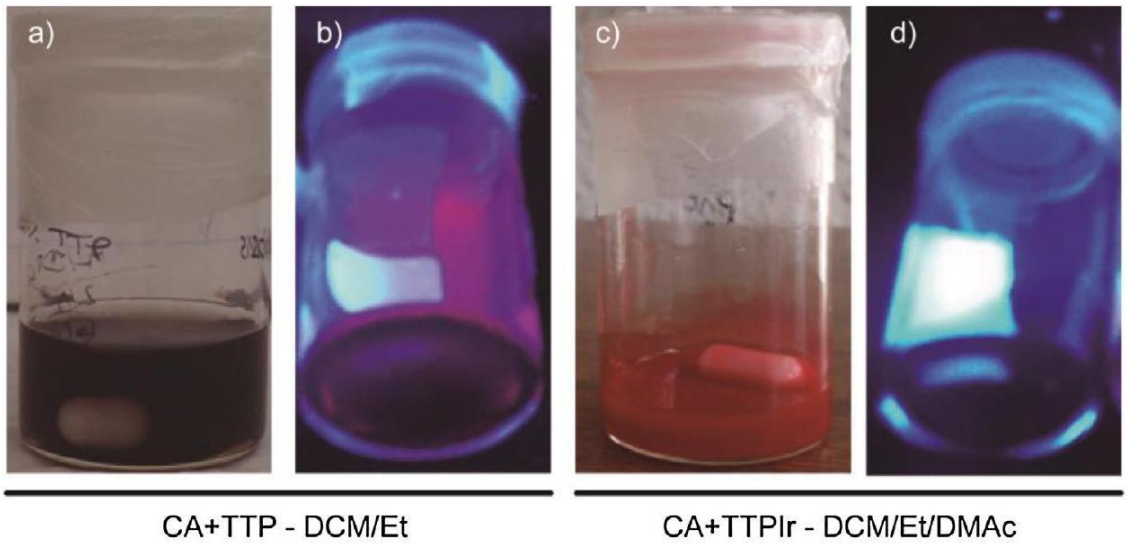

Fig. 2. Spinning solutions at daylight (a and c) and under UV radiation (b and d).

Table 2
Hildebrand and Flory-Huggins parameter of CA(DS = 2.5).

Solvent [b]	d$(MPa^{1/2})$[a]	Flory-Huggins parameter (c)
Dichloromethane [b]	20.2 [b]	- [d]
Ethanol [b]	26.2 [b]	- [d]
Dimethylacetamide [b]	22.5 [c]	0.28
Chloroform [c]	18.8 [c]	0.34
Methanol [c]	29.3 [c]	1.87
DCM/Et	21.4	- [d]
DCM/Et/DMAc	21.5	_ [d]

a SI units.
[b] From Hansen [39] and Barton [35].
[c] From Ghorani[34].
[d] No data available.

The solution prepared using DCM/Et solvent system with CA and TTP showed a fine purple suspension and fluorescence when excited with a 365 nm wavelength (Fig. 2). This solution was used successfully to obtain electrospun membranes. However, the same solvent system with the metallated porphyrin (TTPIr) was unsuccessful. Therefore, to the previous solvent system was added DMAc, a less volatile solvent with a higher boiling point [26,37] and also a higher dielectric constant ($Tb = 166.0°C, e = 37.8$) comparing to the DCM ($Tb = 39.8°C, e = 8.9$) and Et ($Tb = 78.4°C, e = 24.55$) solvents [26]. The obtained solutions with the TTPIr porphyrin were red colored and homogeneous, although the fluorescence was quenched, due to the incorporation of the metal into the porphyrin (Fig. 2).

The rheological behavior and the surface tension of the electrospinning solutions were investigated to study the influence of the porphyrins incorporation in the CA and to help to define the electrospinning parameters.

As demonstrated in Fig. 3 the system of solvents employed show a strong influence in the presented flow curves. The different rheological behavior between the two systems of solvents can be due to its capacity to dissolve CA as a consequence of the solvents ratio used. The solvent system A, which showed a higher viscosity, is composed by 80wt% of a CA solvent, dichloromethane and 20wt% of a non-solvent, ethanol, while, the solvent system B, which presented a lower viscosity, is composed by a higher ratio of the CA solvent (both DCM and DMAc) 90wt% respectively, and only 10wt% of the non-solvent ethanol. Therefore, solvent system B has higher capacity to dissolve CA, which results in lower viscosity. This effect is even more pronounced when the CA concentration increases from 10 to 12wt%. Although, and as it is known the effect of increasing viscosity with increasing polymer concentration [26], the solvent system A shows a more pronounced viscosity increase compared to solvent system B, which again arises from its lower capacity to dissolve CA. The incorporation of the metallated porphyrin, TTPIr, into the system promoted a viscosity decrease, explained by an easier chain alignment when the shear stress is applied. This could result from the higher capacity of TTPIr to disperse

in this system enabling the formation of a homogeneous solution. In this system, it was also observed an approximation of a Newtonian fluid rheological behavior, where the viscosity is almost independent of the shear rate. These effects can be mainly attributed to the addition of the metallated porphyrin, once the same solution prepared with the non-metallated porphyrin did not show this tendency and the same viscosity was kept for CA solution for lower shear rates. Furthermore, the introduction of the non-metallated porphyrin in the system did not show a significant variance on the viscosity compared with CA.

The surface tension of the solutions is quite important for the fibers projection during electrospinning process and it is more likely a function of the solvent system than the polymer concentration [33]. Fig. 4 shows the surface tension of the prepared solutions, being the measurements taken at 15 s and 30 s , after the deposition of the solution on the equipment. The introduction of DMAc on the solvent system A, DCM/Et did not promoted a significant variation on the surface tension of the solutions, probably due to the small amount of DMAc added.

The incorporation of both porphyrins in the system lead to a slight decrease of surface tension, which is more pronounced for the non-metallated porphyrin (TTP), i.e., the latter turns out to be easier to electrospun, since the applied electric field necessary to overcome the surface tension and to obtain nanofibers is lower. In practice this slightly difference was reflected in a potential adjustment needed to electrospun the solutions prepared with the TTP from 16 kV to 20 kV with TTPIr. This is also reflected in the flow rate from 0.1 to 0.5 mL/h, respectively and consequently to a higher mass throughput that resulted in a reduction of the electrospinning time from 60 to 10 min (Table 1).

Properties of the electrospun membranes

The infrared absorption spectra of TTP, TTPIr porphyrins and the cellulose acetate membrane are presented in Fig. 5.

FTIR spectrum of the cellulose acetate membrane with 12wt% – (A) is similar to the spectrum of CA raw material. Moreover, membranes prepared with the system of solvents *A* and *B* are identical revealing that the electrospinning did not promote any chemical changes in the polymer. Thus, in Fig. 5 it is possible to identify the main characteristic bands of cellulose acetate, which are supported by various studies [29,40-45]. A broad band at

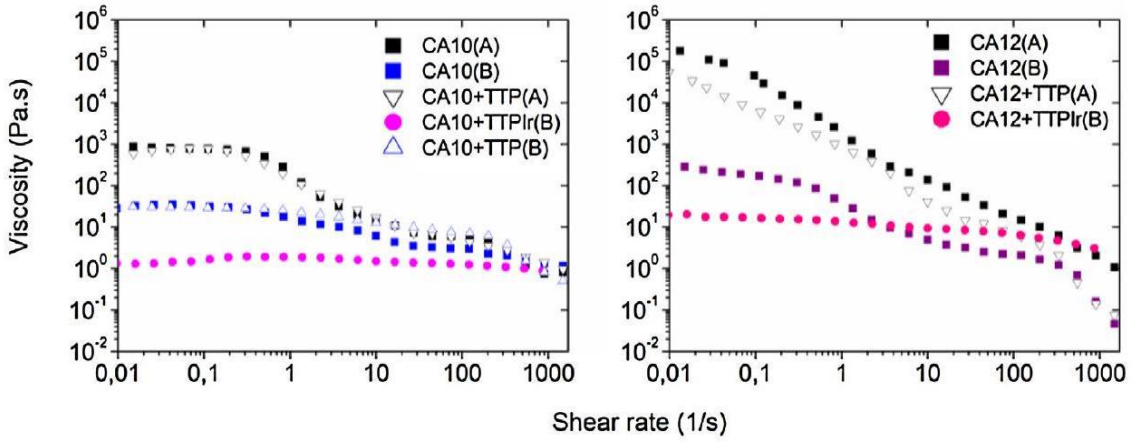

Fig. 3. Flow curves of the electrospinning solutions.

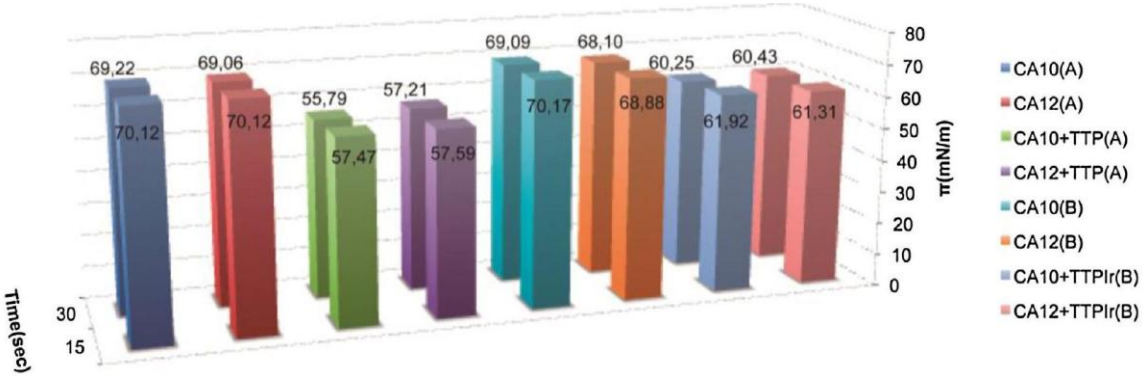

Fig. 4. Surface Tension (p) of the spinning solutions.

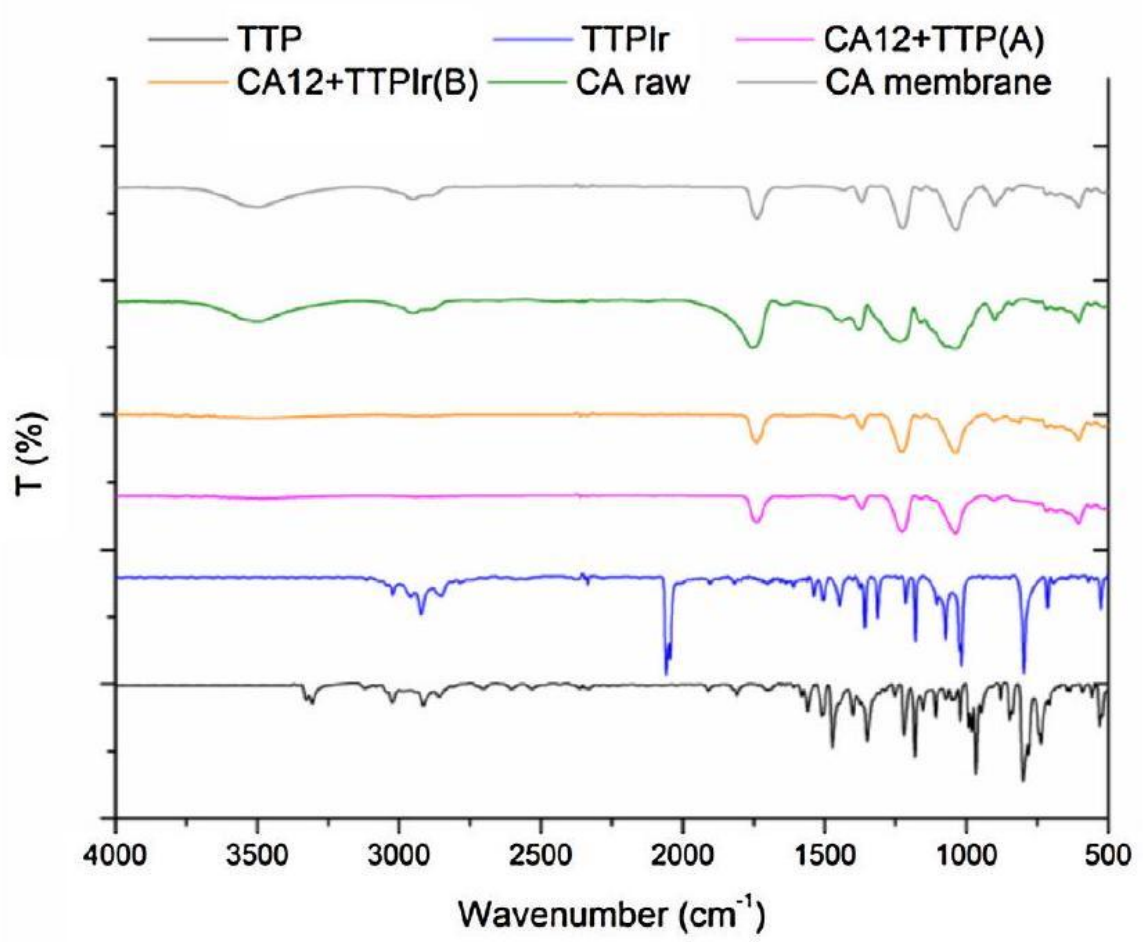

Fig. 5. FTIR spectra of CA raw and membrane, electrospun membranes of CA with the respective porphyrins (TTP and TTPIr), TTP and the respective metalloporphyrin TTPIr.

3471 cm^{-1} that corresponds to the hydroxyl group (OH) stretching, a sharp and strong intensity band at 1741 cm^{-1} that corresponds to the symmetrical stretching and a weak band at 1621 cm^{-1} assigned to the asymmetrical stretching of the ester groups (carbonyl, $C = 0$) are identified. The weak intensity bands at 2870 and 2933 cm^{-1} are assigned to the $C - H$ stretching vibrations of the CH_2 and CH_3 groups, while the 1370 cm^{-1} band to the $C - H$ bending. The $C - O$ stretching was observed as a strong intensity band at 1216 cm^{-1}, as well the $C - O$ symmetric stretching of the primary alcohol at 1025 cm^{-1}. The $C - O - C$ asymmetrical stretching is assigned as a weak band at 1136 cm^{-1} and the band at 895 cm^{-1} is assigned to the b-glucosidic linkages between sugar units that form the polymeric chain of cellulose acetate. From Fig. 5 it is clearly observed the successful metallation of the TTPIr by the absence of the N-H stretching band between 3300 and 3293 cm^{-1} and of a sharp peak at 740 cm^{-1} associated with $N - H$ out-of-plane deformations (these peaks are only present in the free-base TTP porphyrin) [46]. Also, only on the metallated porphyrin is observed a sharp band at 2044 cm^{-1} that could correspond to one of the axial ligands (-CO, carbon monoxide). The bands at $3025 - 3000\ cm^{-1}$ and $2910 - 2800\ cm^{-1}$ are associated to the $C - H$ stretching of the phenyl groups and the later to the $C - H$ stretching of the methyl groups (aliphatic hydrogens), and the peak at 1179 cm^{-1} is associated with the stretching of the $C - H$ of the pyrrole [46].

Regarding the spectra of the membranes with the porphyrins (Fig. 5), the main bands of cellulose acetate previously discussed are easily identified, while the porphyrins correspondent bands are not detected due to a lower incorporation of porphyrins compared to the CA. In order to complement the information collected by FTIR spectra, Raman spectroscopy was performed in the same compounds with a laser of 532 nm wavelength, which permitted a clear identification of the incorporated porphyrins on the CA membranes (Fig. 6). It is also noteworthy that Raman spectra were performed mostly in the fingerprint zone, where it is clearly observed that the incorporation of the iridium atom and the axial ligands had a strong influence in the bonds vibrations of the porphyrin molecule.

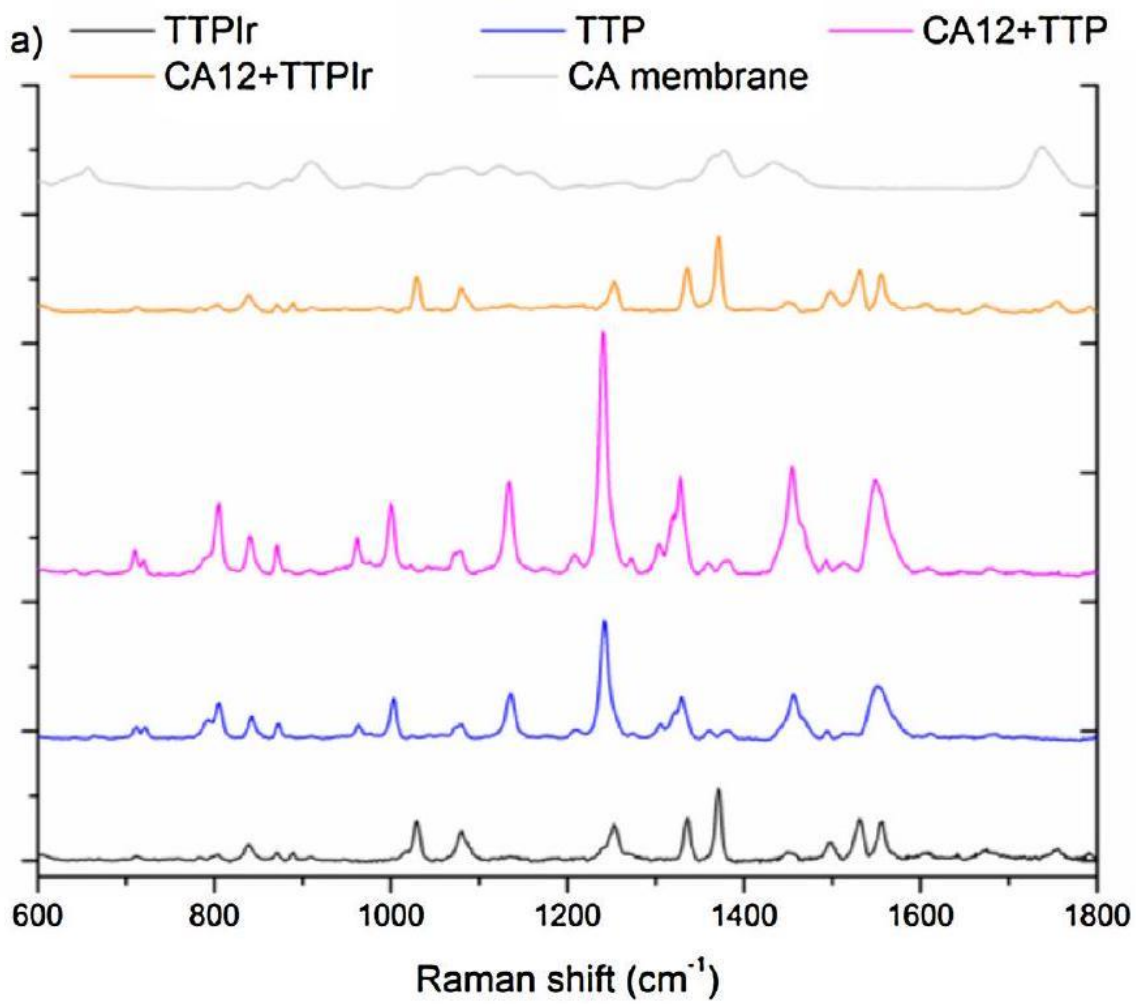

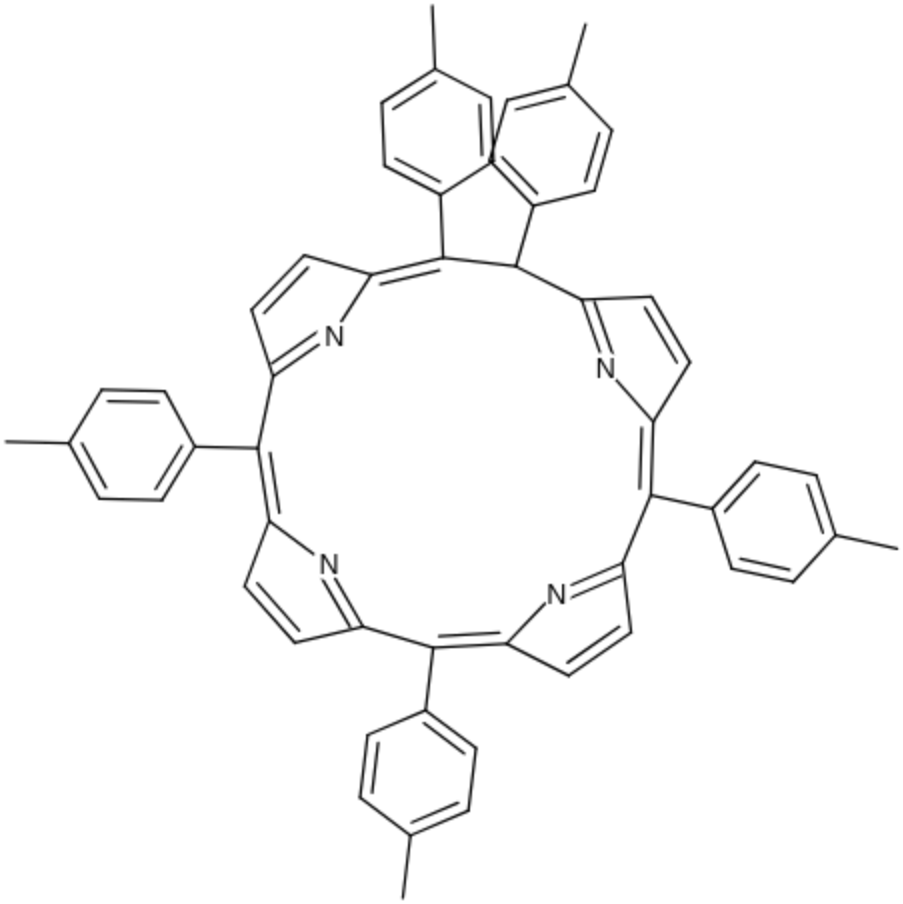

Fig. 6. (a) Raman spectra of CA membrane, electrospun membranes of CA with the respective porphyrins (TTP and TTPIr), TTP and the respective metalloporphyrin TTPIr. (b) Structure of TTP.

Concerning the polymer, the main bands are identified on the electrospun CA membrane (Fig. 6) [47-50]. The 1733 cm^{-1} band is ascribed to the carbonyl ($C=O$) stretching vibrations in the acetyl groups, while the vibrations of the CH_3 groups within the acetyl groups are identified as a shoulder at 1363 cm^{-1} and at 1449 cm^{-1}. The band at 1377 cm^{-1} has correspondence to the various deformations of the cellulose backbone $d(CH_2), d(HCC), d(HCO)$ and $d(COH)$. Between $1300-1000$ cm^{-1} region it is observed the signals of the asymmetric vibrations of CC and CO bonds of the cellulose backbone (1164 cm^{-1}) and the symmetric ring vibrations (1097 cm^{-1} and 1121 cm^{-1}) and ring stretching (1041 cm^{-1} and 908 cm^{-1}) of COC groups. At lower Raman shifts it is observed the vibrations of the bonds within CH_3CO acetyl groups, particularly the deformation vibrations $d(COO)$ at 655 cm^{-1} and 601 cm^{-1}.

Regarding the porphyrin, the bands between 1400 and 1660 cm^{-1} are usually assigned to the stretching frequencies of $C_b - C_{b'}$ and $C_a - C_m$ bonds and the region between 1300 and 1450 cm^{-1} is usually attributed to the stretching motions of the bonds $C_a - C_b$ and $C_a - N$ (Fig. 6) [51,52]. Therefore, from both porphyrins spectra the bands at 1552 cm^{-1} (TTP) and 1557 cm^{-1} (TTPIr) can be attributed to the $C_b - C_{b'}$ bond stretching, symmetric

stretching of $C_a - C_m - C_{a'}$ bonds and the bending formation of $C_a - N(H) - C_{a''}/C_a - N - C_{a'}$ bonds (only for TTP) including rocking of the hydrogen atoms on the $C_{b'}$ atoms [53]. It is possible to observe some differences between the porphyrins in this region, since the nitrogen (N) atom and consequently the bond vibrations are changed due to the presence of the iridium atom. The bands that are identified in both porphyrins at 1080 cm^{-1} could be assigned to the rocking of the hydrogens in the carbon atoms (C_b) in the macrocycle and the band at 1136 cm^{-1} only observed for TTP could be assigned to the rocking of the hydrogen atoms on nitrogen atoms, it can also be assigned to the symmetric stretching of the $C_m - C_a - C_b$ bonds [53]. Moreover, it is of great importance to mention the absence of the band at 963 cm^{-1} in TTPIr, which could be assigned to the $NH - NH$ bonds, and as expected, it is only identified at the nonmetallated porphyrin - TTP [53]. The bands at $900 - 1400$ cm^{-1} are assigned to the stretching vibrations of C_aC_b/C_aN [52].

The Raman spectra of electrospun membranes of cellulose acetate with porphyrins are also showed in Fig. 6(a), where due to the stronger signals of the porphyrins when compared to CA, it is only possible to identify the peaks correspondent to the porphyrins although the nanofibers were prepared with the CA polymer. Therefore, the CA signal in the wavelength range must have a very low intensity. Moreover, the presence of the porphyrins in the membrane was confirmed and no chemical reaction had occurred with the polymer, since new bands are not identified. Also, the porphyrins main characteristic bands are identified in the membrane with TTP and TTPIr (Fig. 6).

The steady-state fluorescence emission at a 532 nm wavelength excitation and the fluorescence imaging of the electrospun membranes are observed in Fig. 7.

Typically the TTP porphyrin is fluorescent as previously mentioned in Fig. 2 for the solutions of electrospinning. Therefore the electrospun membranes were also observed by fluorescence microscopy, and under blue light the membranes show a redyellowish coloration that changes to red when excited with green light (Fig. 7). The emission spectra of membranes shown in Fig. 7d) confirm this result, since the TTP alone or when incorporated with CA and excited at 532 nm wavelength show two main emission peaks located at approximately 660 nm and 720 nm , although a slightly lowering on the peak intensity for CA+TTP is observed, which is related to lower quantity of material analyzed as already observed in the microscope images where it is clear that the porphyrins form small spots into the fibers. A significance lowering on the emission intensity of the TTPIr and the CA+TTPIr membrane is observed, which explains why when observing the fluorescence of both membrane or TTPIr alone at microscope no emission is seen. The explanation can be due to the incorporation of the iridium metal and the axial ligands Cl and CO that formed a stable complex without charge, which quenched the fluorescence of the metalloporphyrin. This effect was also observed in other porphyrins with transition metals such as copper, cobalt and nickel, and can be mainly attributed to the heavy metal effect that relies in the enhancement of strong intramolecular spin-orbit interactions by the metal ion [54-59]. Sherman et al. [60] observed the reduction on fluorescence lifetime promoted by the interaction between a porphyrin and $IrO_2 \cdot nH_2O$ particles. The author assigned the quenching to one or the combination of the possible effects, quenching by energy transfer, electron transfer or by the enhancement of the intersystem crossing [60]. Koren et al. [61,62] also showed that the

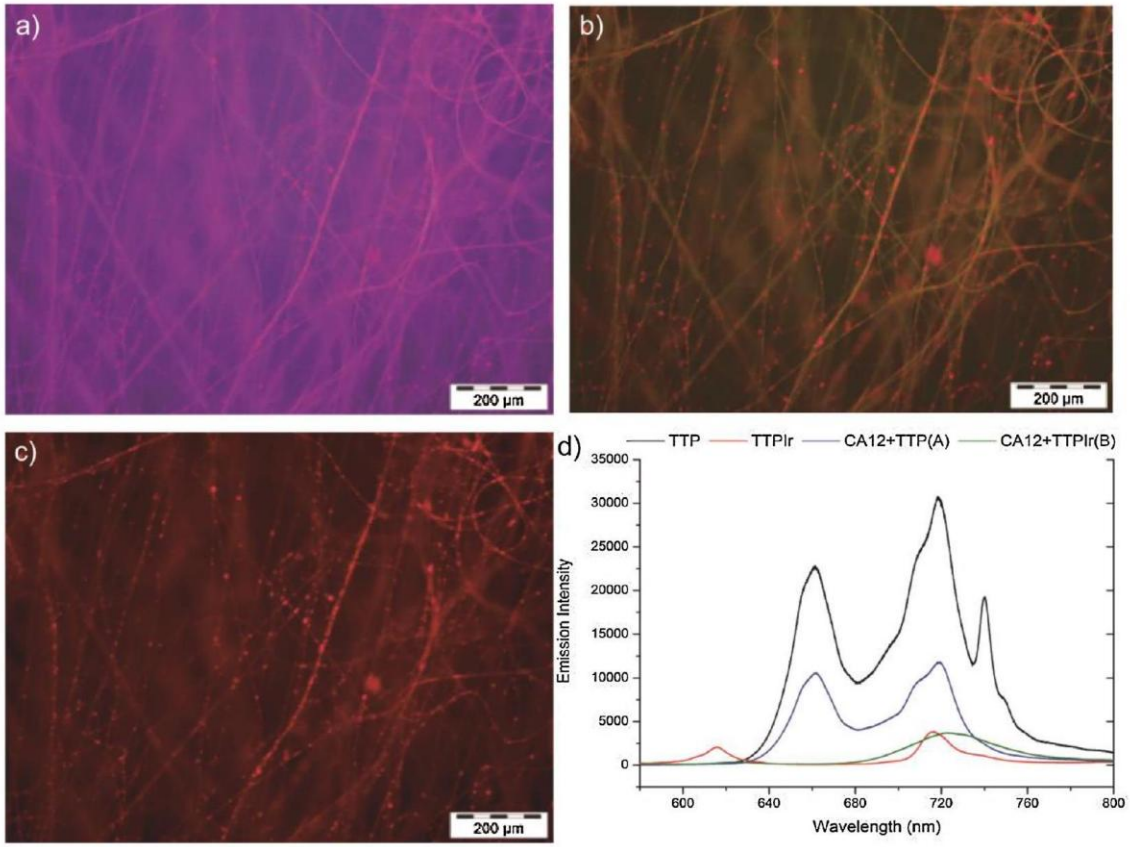

Fig. 7. Fluorescence imaging of the electrospun membranes prepared with 12wt%CA and TTP with the respective wavelengths (a) UV 360 – 370 nm; (b) Blue 460 – 490 nm; (c) Green 510-550 nm and (d) Emission spectra of TTP, TTPIr and CA electrospun membranes with porphyrins excited with 532 nm wavelength. fluorescence of the Ir(III)-octaethylporphyrin could be changed by binding different axial molecules.

The thermal stability of both porphyrins, polymer and the electrospun membranes were studied by thermogravimetric analysis (Fig. 8).

As expected the TTP porphyrin showed a high thermal stability of 484°C. Similarly to others metalloporphyrins, such as, the metaltetraphenylporphyrin, TTPIr shows two onset temperatures [63]. The first at a lower temperature (381°C), which corresponds to the tolyl group or hydrogen atoms release and the second at approximately 523°C due to the degradation of the porphyrin skeleton. The incorporation of both porphyrins into the CA matrix showed an enhancement of the thermal stability of the polymer. This result is expected since the thermal stability of the porphyrins is much higher than the polymer. However, the amount of incorporated porphyrin is not enough to make a significant difference between CA membranes incorporated with TTP and TTPIr.

Fig. 9 shows the SEM microstructures of the unload and loaded CA electrospun membranes with porphyrins from solutions with a polymer concentration of 12wt% in DCM/Et(A) and DCM/Et/DMAc(B) solvent system. Since the morphology of the membranes prepared with either the CA concentration of 10 or 12wt% are identical, only the results with 12wt. % are presented. Therefore, these micrographs are representative of

each sample, where a general overview of the nanofibers is given with a magnification of 1000 × (scale 100 mm) and a more detailed picture is observed with a 10000 × (scale 10 mm) magnification.

Table 3
Fiber mean diameter.

Membranes	Fiber diameter (mm)[a]	Membranes	Fiber Diameter (mm)[a]
CA10(A)	1.2 ± 0.3	CA12(A)	1.6 ± 0.2
CA10(B)	0.7 ± 0.2	CA12(B)	0.9 ± 0.3
CA10+TTP(A)	1.0 ± 0.2	CA12+TTP(A)	1.2 ± 0.1
CA10+TTPIr(B)	0.5 ± 0.1	CA12+TTPIr(B)	0.7 ± 0.2

[a] Mean fiber diameter.

SEM micrographs (Fig. 9) and diameter analysis (Fig. 10 and Table 3) of the fibers, indicate that increasing the CA concentration from 10 to 12wt% resulted in solutions with higher viscosity and membranes with thicker nanofibers. This is a consequence of higher polymer chain entanglements and the overlapping between polymer chains in the solution, which is essential to maintain the continuity of the jet during the electrospinning process [25,33]. The introduction of DMAc into the solvent system promoted a strong reduction of the fiber diameter. The same effect was observed with the incorporation of the porphyrins however, it was more evident on the nanofibers with the metallated porphyrin (TTPIr). The observed reduction of the fibers diameter is related with the viscosity decrease of the spinning solutions previously shown (Fig. 3). Therefore, in all cases, solutions with higher viscosity resulted in membranes with thicker nanofibers [25,26,64-66]. Small agglomerates with diameters between 2 and 3 mm were observed only for the membranes prepared with the porphyrin TTP (Fig. 9). These

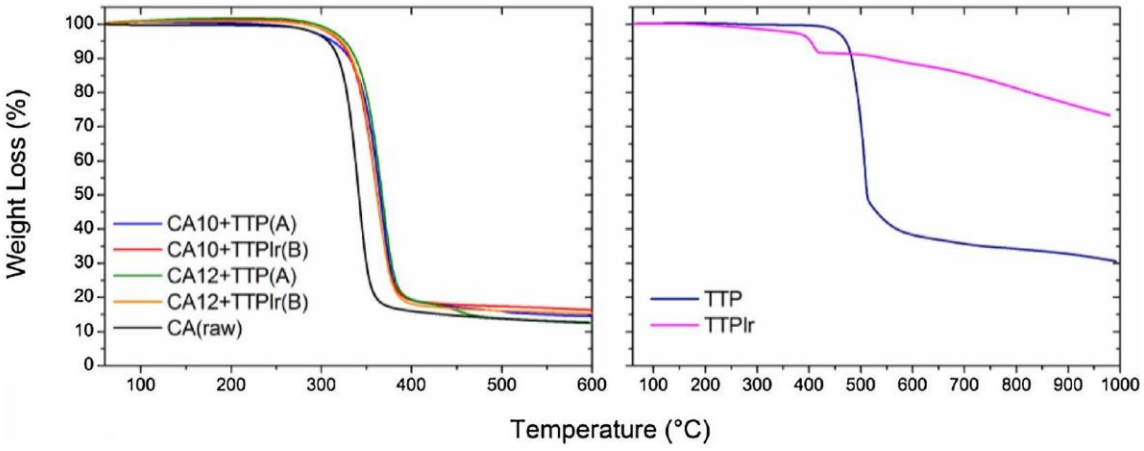

Fig. 8. TGA onset temperature of the porphyrins, raw CA and electrospun membranes.

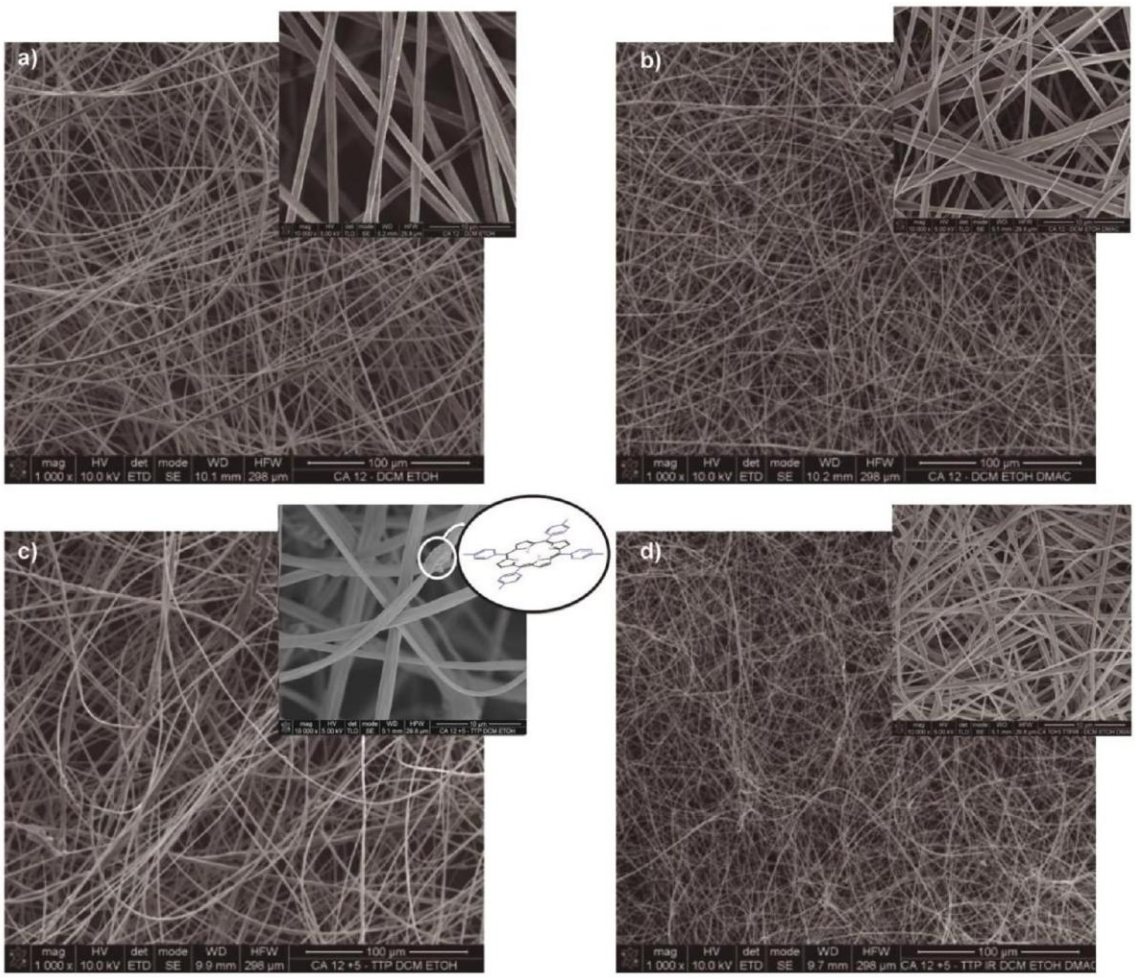

Fig. 9. SEM images of electrospun membranes. a) CA in DCM/Et(A); b) CA in DCM/Et/DMAc (B); c) CA+TTP in DCM/Et (A); CA+TTPIr in DCM/Et/DMAc (B).

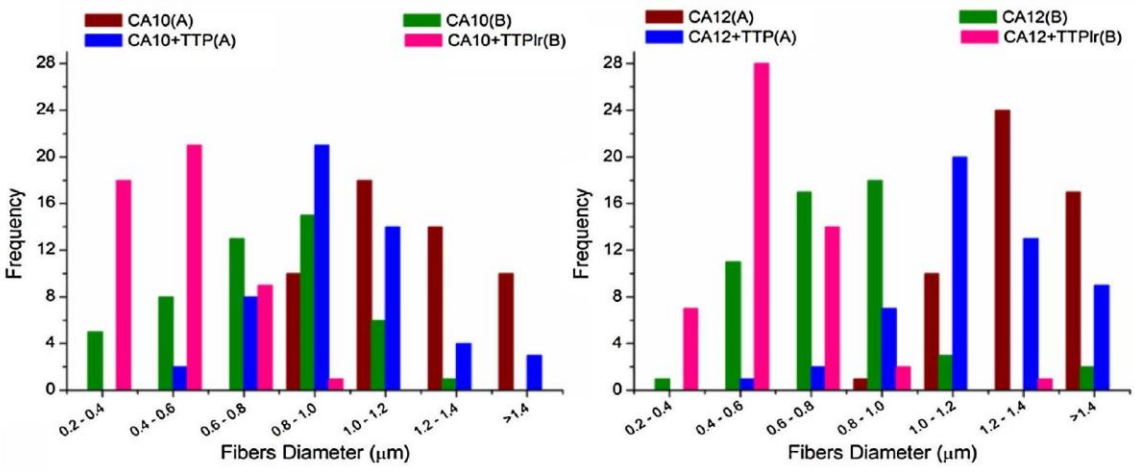

Fig. 10. Average fibers diameter and fibers distribution.
were not considered beads but instead porphyrins agglomerates, which were already

observed by fluorescence microscopy (Fig. 7). This was an expected consequence of the CA+TTP solution suspension previously observed (Fig. 2), where the strength of the relative forces between porphyrins showed to be higher than with the solvent leading to particle clumping [67]. Also, hydrogen bonding between the nitrogen (N) atoms of the core and the hydrogens of the tolyl groups of near porphyrins can lead to porphyrin stacking and agglomeration. The introduction of the iridium and axial ligands into the porphyrin core seems to avoid the formation of this kind of bonding between porphyrins when incorporated in a CA solution, which was reflected in the absence of agglomerates and a uniform distribution of the metallated porphyrin (Fig. 9).

As it can be observed in Fig. 10, fiber diameter of membranes prepared with the solvent system A, DCM/Et is independent of CA concentration, indicating a distribution skewed to the left (i.e., most of the data is concentrated on the right of the figure), which is associated with larger diameters. While the opposite scenario (distribution skewed to the right) is observed with the membranes prepared with B, DCM/Et/DMAc system, confirming the thinning effect induced by the presence of DMAc.

The conductive along the fibers of membranes with porphyrins were analyzed by atomic force microscopy (AFM) both in KFM and CFV mode, while the polymer matrix was only analyzed in CFV mode (Fig. 11). The samples with 12wt% of CA were chosen since no significant changes were observed in the membranes properties prepared with 10 and 12wt% of CA.

AFM images of CA electrospun nanofibers in CFV mode show linear fibers with bundles of strings with a thickness of few hundreds of nanometers to 2 micrometers (Fig. 11(a-c)). Such difference could be a result of the difficulty in performing analysis with electrospun nanofibers, since flat surfaces are preferable. Concerning the KFM analysis, since no current could be established through the membrane with the TTP porphyrin, only images of the surface potential are showed, Fig. 11(d). These revealed clear differences among fibers, where blue corresponds to a lower potential and blue/white up to 1 V higher. Therefore, the darker domains observed on the top left could correspond to the TTP agglomerates observed by SEM and fluorescence microscopy (Figs. 7 and 9), while the remaining CA fiber show clearly a more homogeneous distribution of the surface potential. It seems that the presence of TTP agglomerates prevents/inhibits the establishment of a current circuit and therefore conductive properties. A change of few mV of potential through the fiber membranes was detected for the metallated porphyrin, probably due to the incorporation of the iridium on the porphyrin, which, as expected, promoted a more uniform distribution of the porphyrins on the CA fibers (Fig. 11(e)). It was also observed a slightly higher potential on the fibers comparing with surroundings. Additionally, this was the only sample where it was possible to acquired current image mapping, where highly conductive regions are showed as white/peak domains (approximately 12 nA maximum current) on the large fiber (Fig. 11(f)). Therefore, the establishment of these conductive domains can be a result of the higher dispersed metallated porphyrin, allowing the formation of networked structures with conductive properties. However, it is also observed smaller fibers situated in lower planes that exhibit mostly no conductivity (blue, dark areas). These could be zones of CA nanofibers without porphyrin. The heterogeneity of surface potential and conductive domains showed above can be related not only with the surface chemistry of the analyzed sample, but also with the surface roughness and the presence of voids on the sample, which have a major influence on AFM measurements and can have a strong effect on the results.

A low wettability of membranes can be advantageous for some practical applications, as so the change on the water contact angle (WCA) of the electrospun membranes of CA and CA loaded with porphyrins were also investigated, being the measurements taken at the initial 5 s after water drop and are shown in Fig. 12 with representative photographs. As expected, CA nanofibers has a hydrophobic nature attributed mainly to the presence of the hydrophobic acetyl groups in the polymer structure and to the membrane nanofibers morphology [68,69]. From literature, cellulose triacetate, which has a higher acetyl content of 50% prepared by electrospinning showed a WCA of 141°, while deacetylated cellulose acetate could show lower WCA ranging 0.4° [68,70,71].

CA mats obtained from the solutions with the solvent system B has a consistent higher WCA value (Fig. 12), which is mainly related with thinner nanofibers observed by SEM (Fig. 9) [72,73]. The reduction of the fiber diameter, which were already observed by Ma et al. [72,73] for PCL membranes, can develop hierarchical structures where the surface roughness are known to dramatically increases, as well as the fraction of contact area of the water droplet with the air trapped in the spaces between increasing the hydrophobicity of the respective membrane. Since, the WCA angle is inversely related to hydrophilic properties, it means that the higher contact angles presented lead to more hydrophobic mem-

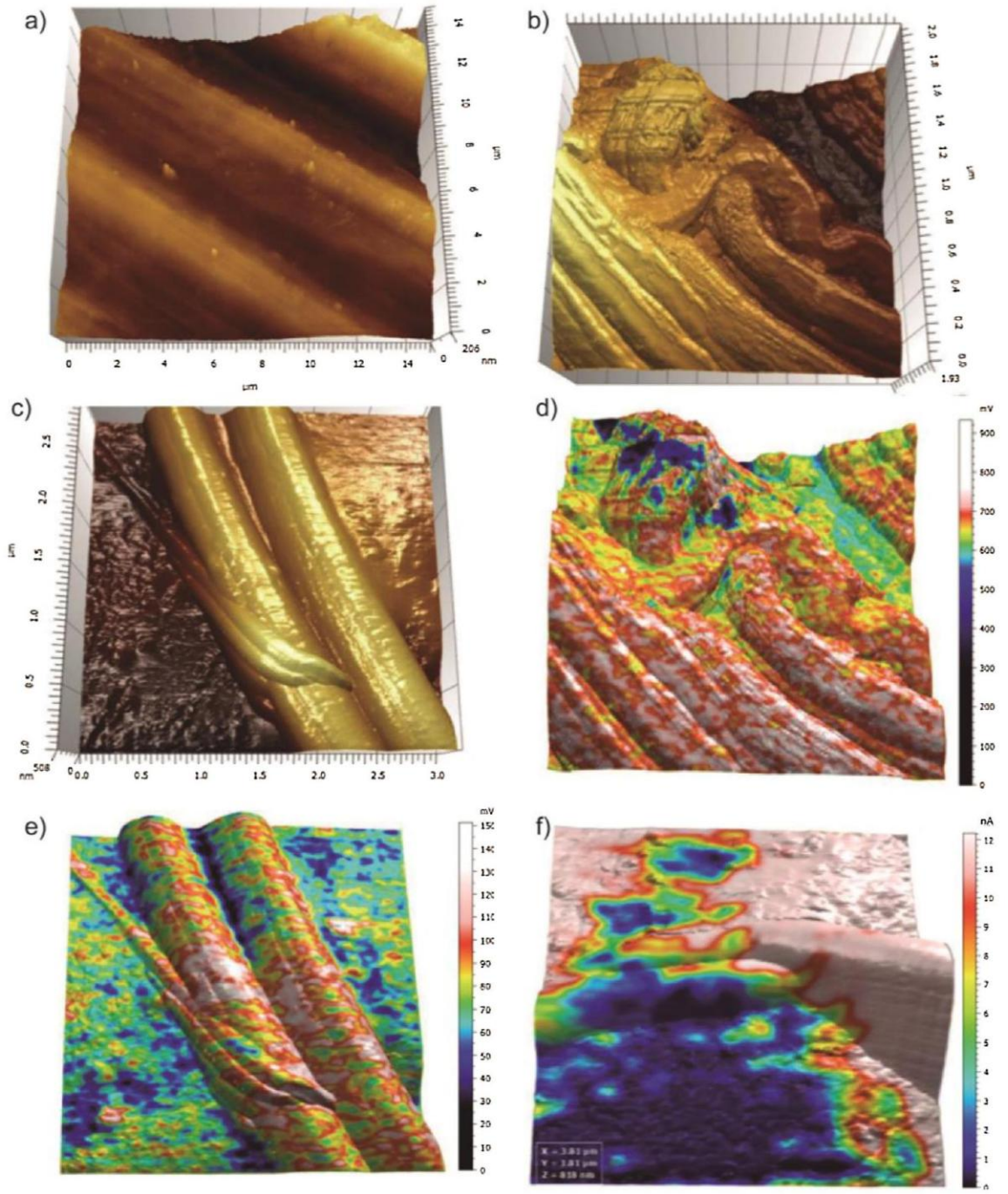

Fig. 11. AFM images of electrospun membranes, topography analysis: (a) CA12 wt% (15 mm scan); (b) CA12 + TTP (2 mm scan); (c) CA12 + TTPIr (2 mm scan); surface potential: (d) CA12 + TTP (2 mm scan) and (e) CA12 + TTPIr (3 mm scan) and current image: (f) CA12 + TTPIr (4 mm scan).

branes [74,75]. Electrospun membranes containing porphyrins depicted a slightly increase on hydrophobicity, which it was already expected since both porphyrins are water-insoluble and only a small amount was incorporated. However, according to Ma. M [72,73] it could be expected a wider WCA enhancement of the membranes with agglomerated TTP, similar to the membranes with micro-beaded fibers, such higher WCA was not observed. Instead,

the thinner and uniform fibers obtained from the membranes with TTPIr showed higher WCA values, which are related with increasing of the surface roughness, once thinner nanofibers can trapped more air in between. Thus, it is noteworthy that WCA is not only affected by the polymer chemical structure but also by other parameters, such as porosity and roughness of the fibers web [68]. From literature CA films prepared by different methods as phase inversion

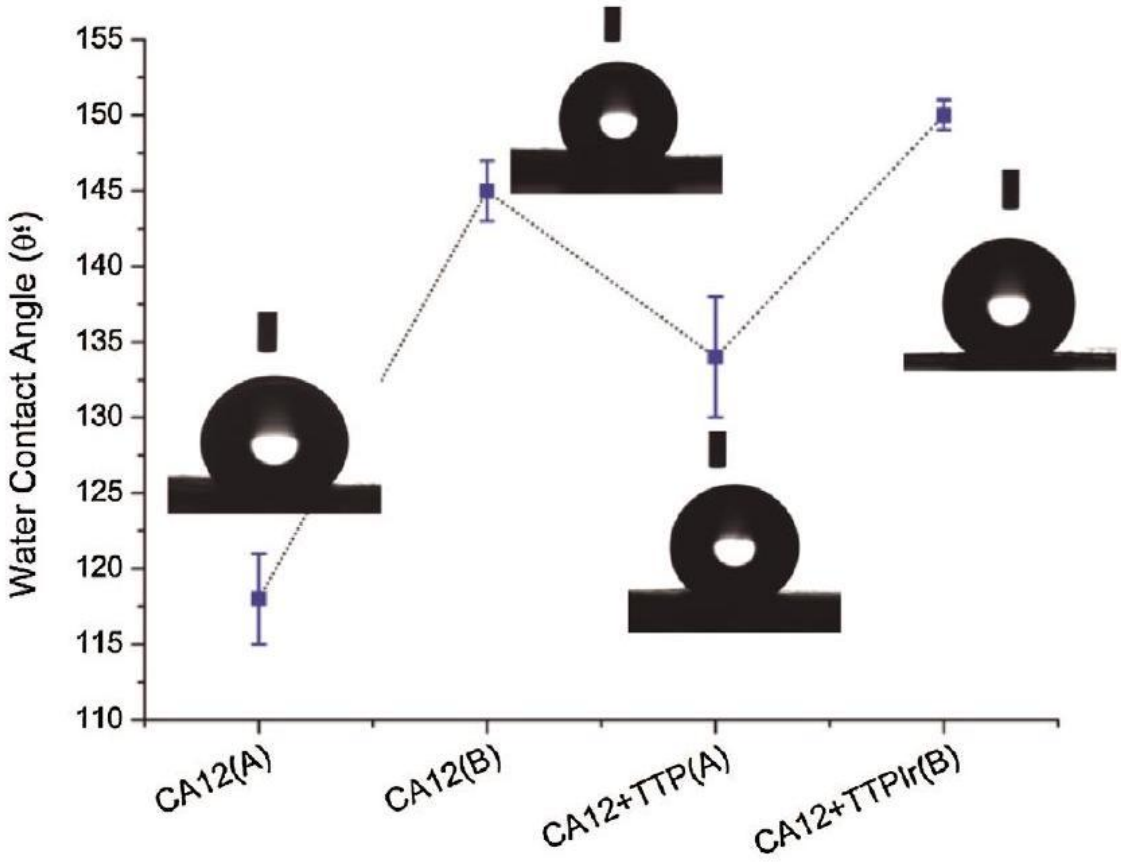

Fig. 12. Water Contact Angle of electrospun mats of CA and CA loaded with porphyrins and representative water droplet photographs.

or solution casting have lower WCA compared to electrospun CA membranes. Since the electrospinning technique permits the trapping of more air (between fibers) under the falling water droplet enhancing the WCA value [74,76,77]. Also, depending of the solvent system employed and the electrospinning conditions, the fiber morphologies differ affecting the WCA results [37,72,77,78].

Conclusions

Cellulose acetate electrospun nanofibers were successfully prepared with the solvent systems DCM/Et(A) and DCM/Et/DMAc (B). The first system of solvents A, showed to be suitable for the preparation of CA nanofibers with the non-metallated porphyrin, TTP, but it needs small amount of DMAc to optimize the electrospinning process for metallated porphyrin, TTPIr. The solutions obtained from the system DCM/Et with the TTP showed to be purple with visible suspensions resulting in the formation of fibers with

agglomerates, while the system DCM/Et/DMAc with the TTPIr showed a red homogeneous solution with an efficient porphyrin dispersion and smooth and thinner fibers. The diameter reduction was observed to be a consequence not only of the introduction of the DMAc solvent but also of the metallation of the TTP. The main absorption bands of the porphyrins and CA polymer were identified by FTIR and Raman spectroscopy and proved the incorporation of porphyrins into the CA membranes. Moreover, microscopy fluorescence has shown red luminescence of nanofibers with TTP under the excitation wavelength of blue and green light, although agglomerates of porphyrins when incorporated exhibited no electrical conductivity. Whereas, the nanofibers prepared with the TTPIr showed a lower emissivity but higher electrical conductivity as conductive paths can be established due to a more uniform distribution inside the membrane. The surface properties of the nanofibers were also improvement in hydrophobicity when the porphyrins were incorporated.

Acknowledgements

The authors acknowledge the Portuguese Foundation of Science and Technology (SFRH/BD/81711/2011 and PEstC/CTM/LA0025/2011) and n-STeP - Nanostructured Systems for Tailored Properties, with reference NORTE-07-0124-FEDER000039, supported by the Programa Operacional Regional do Norte (ON.2).

References

[1] S. Agarwal, A. Greiner, J.H. Wendorff, Prog. Polym. Sci. 38 (2013) 963-991.
[2] Z. Dong, S.J. Kennedy, Y. Wu, J. Power Sources 196 (2011) 4886-4904.
[3] T.P. Wijesekera, D. Dolphin, Metalloporphyrins in Catalytic Oxidations, 1994, pp. 193-239, Chapter 7.
[4] R. Giovannetti, The use of spectrophotometry UV-vis for the study of porphyrins, in: J. Uddin (Ed.), Macro to Nano Spectroscopy, InTech, 2012.
[5] W. Zheng, N. Shan, L. Yu, X. Wang, Dyes Pigm. 77 (2008) 153-157.
[6] M.-S. Liao, S. Scheiner, Chem. Phys. 285 (2002) 195-206.
[7] Z. Valicsek, O. Horváth, Microchem. J. 107 (2013) 47-62.
[8] D.Y. Seong, M.-S. Choi, Y.-J. Kim, Eur. Polym. J. 48 (2012) 1988-1996.
[9] J. Mosinger, K. Lang, L. Plistil, S. Jesenska, J. Hostomsky, Z. Zelinger, P. Kubat, Langmuir 26 (2010) 10050-10056.
[10] M.T. Takuma Arai, Hiroyoshi Kawakami, Applied Materials Interface 4 (2012) 5453-5457.
[11] Y.-Y. Lv, W. Xu, F.-W. Lin, J. Wu, Z.-K. Xu, Sens. Actuators B 184 (2013) 205-211.
[12] Y.-Y. Lv, J. Wu, Z.-K. Xu, Sens. Actuators B 148 (2010) 233-239.
[13] Y. Long, H. Chen, H. Wang, Z. Peng, Y. Yang, G. Zhang, N. Li, F. Liu, J. Pei, Anal. Chim. Acta 744 (2012) 82-91.
[14] S. Yan, Z. Nai-qian, W. Miao, Y.C. -q, Qing-biao Zhang, W. Heng-guo, L. Yao-xian, Chem. Res. Chin. Univ. 24 (2008) 722-725.
[15] Y. Jin, X. Lu, C. Wang, J. Appl. Polym. Sci. 102 (2006) 6017-6022.
[16] R. Xue, C. Ge, K. Richardson, A. Palmer, M. Viapiano, J.J. Lannutti, ACS Appl. Mater. Interfaces 7 (2015) 8606-8614.
[17] C. Wolf, M. Tscherner, S. Köstler, Sens. Actuators B 209 (2015) 1064-1069.
[18] Y.-Y. Lv, J. Wu, L.-S. Wan, Z.-K. Xu, J. Phys. Chem. C 112 (2008) 10609-10615.
[19] L. Shao, J. Chen, L. He, G. Xing, W. Lv, Z. Chen, Q. Chenze, Turk. J. Chem. 36 (2012)

700-708.
[20] J. Suchanek, P. Henke, J. Mosinger, Z. Zelinger, P. Kubat, J. Phys. Chem. B 118 (2014) 6167-6174.
[21] P. Henke, K. Lang, P. Kubat, J. Sykora, M. Slouf, J. Mosinger, Appl. Mater. Interface 5 (2013) 3776-3783.
[22] R. Konwarh, N. Karak, M. Misra, Biotechnol. Adv. 31 (2013) 421-437.
[23] S. Vrieze, T. Camp, A. Nelvig, B. Hagström, P. Westbroek, K. Clerck, J. Mater. Sci. 44 (2008) 1357-1362.
[24] D. Haas, S. Heinrich, P. Greil, J. Mater. Sci. 45 (2009) 1299-1306.
[25] A. Celebioglu, T. Uyar, Mater. Lett. 65 (2011) 2291-2294.
[26] S. Tungprapa, T. Puangparn, M. Weerasombut, I. Jangchud, P. Fakum, S. Semongkhol, C. Meechaisue, P. Supaphol, Cellulose 14 (2007) 563-575.
[27] K.Y. Lee, L. Jeong, Y.O. Kang, S.J. Lee, W.H. Park, Adv. Drug Deliv. Rev. 61 (2009) 1020-1032.
[28] M.W. Frey, Polym. Rev. 48 (2008) 378-391.
[29] Y.E. Greish, M.A. Meetani, E.A. Al Matroushi, B.A. Shamsi, Carbohydr. Polym. 82 (2010) 569-577.
[30] J. Matulevicius, L. Kliucininkas, D. Martuzevicius, Chemija 25 (2014) 125-129.
[31] S.K. Yeung, K.S. Chan, Organometallics 24 (2005) 6426-6430.
[32] N.B. Vargaftik, B.N. Volkov, L.D. Voljak, J. Phys. Chem. Ref. Data 12 (1983) 817.
[33] Z.-M. Huang, Y.Z. Zhang, M. Kotaki, S. Ramakrishna, Compos. Sci. Technol. 63 (2003) 2223-2253.
[34] B. Ghorani, S.J. Russell, P. Goswami, International, J. Polym. Sci. 2013 (2013) 1-12.
[35] A.F.M. Barton, CRC Handbook of Solubility Parameters and Other Cohesion Parameters, CRC Press, 1983.
[36] M. Belmares, M. Blanco, W.A. Goddard 3rd, R.B. Ross, G. Caldwell, S.H. Chou, J. Pham, P.M. Olofson, C. Thomas, J. Comput. Chem. 25 (2004) 1814-1826.
[37] H. Liu, Y.-L. Hsieh, J. Polym. Sci. B: Polym. Phys. 40 (2002) 2119-2129.
[38] M.A. Van Dijk, A. Wakker, Concepts in Polymer Thermodynamics, Taylor & Francis, 1998.
[39] C.M. Hansen, J. Paint Technol. 39 (1967) 505-510.
[40] Z.-T. Liu, X. Fan, J. Wu, L. Zhang, L. Song, Z. Gao, W. Dong, H. Xiong, Y. Peng, S. Tang, React. Funct. Polym. 67 (2007) 104-112.
[41] C. Tsioptsias, K.G. Sakellariou, I. Tsivintzelis, L. Papadopoulou, C. Panayiotou, Carbohydr. Polym. 81 (2010) 925-930.
[42] G. Rodrigues Filho, D.S. Monteiro, C.D.S. Meireles, R.M.N. de Assunção, D.A. Cerqueira, H.S. Barud, S.J.L. Ribeiro, Y. Messadeq, Carbohydr. Polym. 73 (2008) 74-82.
[43] M.d.C.C. Lucena, A.E.V. de Alencar, S.E. Mazzeto, S.d.A. Soares, Polym. Degrad. Stab. 80 (2003) 149-155.
[44] S. Gaan, L. Mauclaire, P. Rupper, V. Salimova, T.-T. Tran, M. Heuberger, J. Anal. Appl. Pyrolysis 90 (2011) 33-41.
[45] H.S. Barud, A.M. de Araújo Júnior, D.B. Santos, R.M.N. de Assunção, C.S. Meireles, D.A. Cerqueira, G. Rodrigues Filho, C.A. Ribeiro, Y. Messaddeq, S.J.L. Ribeiro, Thermochim. Acta 471 (2008) 61-69.
[46] D. Skrzypek, I. Madejska, J. Habdas, Solid State Sci. 9 (2007) 295-302.
[47] K. Zhang, A. Feldner, S. Fischer, Cellulose 18 (2011) 995-1003.
[48] K. Schenzel, S. Fischer, Cellulose 8 (2001) 49-57.
[49] H.G.M. Edwards, D.W. Farwell, D. Webster, Spectrochimica acta part a, Mol. Biomol. Spectrosc. 53 (1997) 2383-2392.
[50] V. Rastogi, D. Stanssens, P. Samyn, Materials 7 (2014) 7196-7216.
[51] D.-M. Chen, T. He, D.-F. Cong, Y.-H. Zhang, F.-C. Liu, J. Phys. Chem. A 105 (2001)

3981-3988.
[52] Y.-H. Zhang, D.-M. Chen, T. He, F.-C. Liu, Spectrochim. Acta Part A 59 (2003) 87-101.
[53] M. Aydin, Vib. Spectrosc. 68 (2013) 141-152.
[54] L. Pekkarinen, H. Linschitz, J. Am. Chem. Soc. 82 (1960) 2407-2411.
[55] A. Prodi, C.J. Kleverlaan, M.T. Indelli, F. Scandola, E. Alessio, E. Iengo, Inorg. Chem. 40 (2001) 3498-3504.
[56] M. Rae, A. Fedorov, M.N. Berberan-Santos, J. Chem. Phys. 119 (2003) 2223.
[57] C.M. Drain, J.T. Hupp, K.S. Suslick, M.R. Wasielewski, X. Chen, J. Porphyr. Phthalocyanines 6 (2002) 243-258.
[58] S. Mathai, T.A. Smith, K.P. Ghiggino, Photochem. Photobiol. Sci. 6 (2007) 995-1002.
[59] I. Bouamaied, T. Coskun, E. Stulz, 121, 2006. 1-47.
[60] B.D. Sherman, S. Pillai, G. Kodis, J. Bergkamp, T.E. Mallouk, D. Gust, T.A. Moore, A.L. Moore, Can. J. Chem. 89 (2011) 152-157.
[61] K. Koren, S.M. Borisov, R. Saf, I. Klimant, Eur. J. Inorg. Chem. 2011 (2011) 1531-1534.
[62] K. Koren, R.I. Dmitriev, S.M. Borisov, D.B. Papkovsky, I. Klimant, ChemBioChem 13 (2012) 1184-1190.
[63] O. Ikeda, H. Fukuda, H. Tamura, J. Chem. Soc. Faraday Trans. 1: Phys. Chem. Condens. Phases 82 (1986) 1561-1573.
[64] S.O. Han, J.H. Youk, K.D. Min, Y.O. Kang, W.H. Park, Mater. Lett. 62 (2008) 759-762.
[65] W.K. Son, J.H. Youk, S.T. Lee, H.W. Park, J. Polym. Sci. Part B: Polym. Phys. 42 (2004).
[66] X. Zong, K. Kim, D. Fang, S.H. Ran, S. Benjamin, B. Chu, Polymer 43 (2002) 4403-4412.
[67] R.G. Larson, The Structure and Rheology of Complex Fluids, OUP, USA, 1999.
[68] Z. Khatri, K. Wei, B.-S. Kim, I.-S. Kim, Carbohydr. Polym. 87 (2012) 2183-2188.
[69] H. Liu, C. Tang, Polym. J. 39 (2006) 65-72.
[70] Y.I. Yoon, H.S. Moon, W.S. Lyoo, T.S. Lee, W.H. Park, Carbohydr. Polym. 75 (2009) 246-250.
[71] M.E. Vallejos, M.S. Peresin, O.J. Rojas, J. Polym. Environ. 20 (2012) 1075-1083.
[72] M. Ma, R.M. Hill, G.C. Rutledge, J. Adhes. Sci. Technol. 22 (2008) 1799-1817.
[73] M. Ma, Y. Mao, M. Gupta, K.K. Gleason, G.C. Rutledge, Macromolecules 38 (2005) 9742-9748.
[74] F. Sabeti Dehkordi, M. Pakizeh, M. Namvar-Mahboub, Appl. Clay Sci. 105-106 (2015) 178-185.
[75] Y. Ma, F. Shi, Z. Wang, M. Wu, J. Ma, C. Gao, Desalination 286 (2012) 131-137.
[76] D. Rana, B. Scheier, R.M. Narbaitz, T. Matsuura, S. Tabe, S.Y. Jasim, K.C. Khulbe, J. Membr. Sci. 409-410 (2012) 346-354.
[77] S. Anitha, B. Brabu, D. John Thiruvadigal, C. Gopalakrishnan, T.S. Natarajan, Carbohydr. Polym. 97 (2013) 856-863.
[78] L. Shuiping, T. Lianjiang, H. Weili, L. Xiaoqiang, C. Yanmo, Mater. Lett. 64 (2010) 2427-2430.